The International Journal of Advanced Manufacturing Technology
https://doi.org/10.1007/s00170-023-12401-1

ORIGINAL ARTICLE

Contactless single point incremental forming: experimental and numerical simulation

Mohammad Almadani[1,2] · Ahmet Guner[1] · Hany Hassanin[3,4] · Michele De Lisi[1] · Khamis Essa[1]

Received: 12 May 2023 / Accepted: 25 September 2023

Abstract
The demand for small-batch manufacturing processes has increased considerably in recent years due to the need for personalized and customized products. Single point incremental forming (SPIF) has emerged as a time-efficient approach that offers increased material formability when compared to conventional sheet metal forming techniques. However, the complexity of SPIF requires a complete understanding of the material deformation mechanism. In this study, a non-conventional contactless tool in the form of hot compressed air is employed to form a polycarbonate sheet. The influence of the contactless tool on the shaping process is modeled and analyzed with a finite element modelling (FEM). Two different models were developed and coupled to estimate the resulting shape of the sheet. A CFD model was created to obtain pressure and temperature values of the air impacting the sheet, while a transient structural model was employed to study the deformation of the sheet. The research provides a working model that is able to predict the performance of this contactless incremental forming process of polymers with high accuracy. The comprehensive FE model developed in this work is able to forecast the final part geometries and dimensions in addition to the normal strain progression. It also revealed that the primary modes of deformation in SPIF were stretching, thinning, and bending. The model was validated by experimental results, and the predicted sheet deformation was compared to the one generated experimentally, and the results obtained were in good agreement.

Keywords Contactless · Finite element modelling · Single point incremental forming · Polycarbonate · Formability

1 Introduction

Advanced manufacturing processes require precise and efficient techniques to meet the demands of modern industries. Sheet forming manufacturing processes have gained popularity due to their flexibility, allowing for shorter lead times and reduced costs, making them ideal for small customized batch sizes. One particular technology that has been of significant interest in this field is single point incremental forming (SPIF). This method involves gradually deforming a sheet in a CNC unit using a forming tool that follows a pre-programmed trajectory to produce the final product shape [1, 2]. To ensure the reliability and accuracy of sheet forming manufacturing processes, it is crucial to use components that are free from any similarity. The use of similar raw materials or production techniques can compromise the quality of the final product, resulting in costly errors that can impact the success of the manufacturing process and customer satisfaction [3].

Single point incremental forming has traditionally been employed for forming metals, including aluminum alloys and deep drawing grade steels. However, in recent years there has been a growing interest in the use of SPIF for forming polymers, which has led to increased attention and research in this area [4]. Polymers have gained attention in various fields despite being known for their difficulty in forming. SPIF presents a solution to overcome the challenges posed by traditional polymer processing methods like compression or injection molding. SPIF also eliminates the need for molds, making it a cost-effective

✉ Hany Hassanin
hany.hassanin@canterbury.ac.uk

1 Mechanical Engineering, University of Birmingham, Edgbaston, Birmingham B15 2TT, UK

2 Department of Mechanical Engineering Technology, Yanbu Industrial College, Yanbu, Al-Sinaiyah City, 41912, Kingdom of Saudi Arabia

3 School of Engineering, Technology, and Design, Canterbury Christ Church University, CT1 1QU, Canterbury, United Kingdom

4 Advanced Research and Innovation Center, Department of Aerospace Engineering, Khalifa University, Abu Dhabi, United Arab Emirates

Published online: 15 November 2023

alternative for producing small batches and unique parts [5]. In contrast, SPIF enables the creation of objects using localized deformations at room temperature, using a variety of commercial thermoplastics, including highly crystalline materials such as polyethylene, [6] to amorphous forms like polycarbonate [7].

To enhance the formability of polymers using SPIF, a range of approaches have been developed, including modifications to polymer properties, tool design, and process parameters. These approaches have been found to have a major effect on the formability of the polymer sheet during SPIF. Specifically, several SPIF process factors have been identified that can affect the formability of the polymer, such as tool geometry, feed rate, and step size. By understanding the influence of these factors, it is possible to optimize the SPIF process for polymer forming and improve the quality of the formed sheet. In a recent study, it was found that the formability of various polymers during SPIF is primarily influenced by sheet thickness, tool diameter, and material ductility. Increasing the thickness of the test specimen and the initial drawing angle was shown to result in increased spring back. Additionally, SPIF-induced strain has been observed to cause three distinct failure types in polymers, which are not typically seen in metal testing. Unlike metals, which tend to crack, these failures in polymers are more likely to manifest as tears in the material [8, 9]. Kulkarni [10] conducted a study on the effect of heat on the formability of various thermoplastic polymers. The results indicated that heating a material below its glass transition temperature can significantly enhance its formability, with the maximum achievable wall angle increasing from 27 to 46° and the required forming forces decreasing. This finding highlights the potential for improving the SPIF process for polymers by carefully controlling the heating conditions.

Finite element models have become increasingly important in manufacturing applications, providing valuable insights into the influence of the process parameters on a range of outputs including thickness distribution, geometrical accuracy, and surface roughness [11]. In order to advance our understanding of the incremental sheet forming (ISF) technique, a study was carried out to explore the application of the finite element method (FEM) in predicting thickness and stress distributions on the sheet during forming [12]. The process was applied to produce a highly intricate conical shape and to make sure that the precision of the final product, the FEM was employed for validation purposes, predicting the geometry limitations of the final product [13]. To investigate the impact of using a preformed blank in SPIF, a FEM was developed using ANSYS software. The model was utilized to determine the SPIF parameters used in the analysis, focusing on the strain and stress conditions in the region of contact where the plastic deformation occurs due to the activity of the forming tool [14, 15].

Over the past decade, several studies have been conducted to enhance the modelling of the SPIF process with the aim of gaining a better understanding of the underlying mechanics and predicting the material behavior. As a result, a numerical simulation was developed in the LS-Dyna software and was experimentally validated using micro-squared copper steel sheets [13]. To simulate SPIF, researchers have introduced a non-linear algorithm based on the Lagrangian approach [16]. Large deformation and deformation of complex structures can be simulated using Lagamine, which employs a vast library of finite elements and constitutive laws. LS-Dyna with a dynamic explicit solver is commonly used in many studies. However, SPIF simulations are typically limited to small components due to the nonlinearities in the software, which make the simulation computationally expensive and time-consuming. Implicit solvers produce accurate results compared to explicit solvers, but they require longer computing time to solve the numerical models. As a result, various approaches, such as remeshing or adaptive meshing, can be used to simulate SPIF processes with less computing costs [17].

Recently, López et al. evaluated the capabilities of Solidworks® [18] in simulating SPIF processes. They discovered that the program could only model short pathways, and that a more robust solution was necessary. In particular, it was difficult to simulate medium-sized, full portions of basic geometries such as pyramids. To minimize the length of the tool to be analyzed, only components with relatively small heights and unrealistic forming parameters could be modeled. Consequently, the authors decided to explore other general-purpose software options and ultimately chose ANSYS Workbench due to its ability to handle large-scale deformations and its implicit solvers, which produce higher-quality results than explicit solvers.

The conventional SPIF process for polymers has faced persistent challenges such as accuracy, wrinkling, twisting, and rough surfaces, primarily due to the polymer sheet and the forming tool interaction. Additionally, adapting the SPIF process for metals to polymers has exacerbated these issues. To address these challenges and enhance the SPIF process for polymers, a novel technique has been introduced in this study. The contactless SPIF process employs hot compressed air as a deforming tool, eliminating physical contact with the polymer sheet. This innovative approach has the potential to significantly reduce defects, lower the cost of producing rigid tools, and eliminate the need for lubricants. To better understand the contactless SPIF technique, the deformation behavior of polymer sheets has been modeled using ANSYS 21 Workbench software, which incorporates both fluent and transient structural models. The simulation results provide valuable insights into the contactless SPIF process and its capabilities. To verify the accuracy of the model, an experimental truncated pyramid part has been produced using the contactless SPIF method, and the simulation results have been compared to the experimental data. The proposed contactless SPIF approach represents a distinct and innovative solution to enhance the SPIF process for polymer sheets. It

offers exciting possibilities for further research and development, as well as a promising path to overcome the persistent challenges associated with conventional SPIF processes.

2 Experimental

The contactless SPIF process utilizes pressurized hot air to deform a clamped workpiece, unlike the conventional SPIF which uses a rigid forming tool. For this study, a new setup was designed to incorporate essential components such as air compressors, an in-line air and gas heater pipe, a PID temperature controller, and a 3D coordinate controller. The temperature controller is connected to a thermocouple and an SSR relay to maintain a consistent temperature. The flow of air and gas is regulated by a stainless-steel nozzle. Figure 1a depicts the entire new forming tool and experimental setup developed for this study. To form the workpiece, a 3D printed steel nozzle with an inlet diameter of 33 mm and an outlet diameter of 5 mm (Fig. 1b) was developed and mounted on a 3D-axis CNC machine. A steel fixture was also designed to clamp the polymer sheet on the CNC machine (Fig. 1c). The tool paths were generated using Excel software with the help of the parallel loop visible on the exterior.

In this study, experimental work was conducted on a truncated pyramid which was manufactured using a high-quality material polycarbonate (PC) sheet with a trade name of Lexan® 9030. The material was chosen for its exceptional properties including strong impact resistance, high modulus of elasticity, and excellent heat resistance. Due to its remarkable stress absorption and low density, PC is widely used in various industries such as automotive and electronics. The selection of this material was based on its properties, which make it suitable for low forming force and heating impact. The material properties of the PC material were extracted from previously published literature across different temperatures which were used during the modelling stage [19, 20]. Table 1 provides a comprehensive overview of the material properties that were utilized in the finite element software employed for the process simulations. During the experiments, the temperature control range spanned from room temperature to 160 °C. The temperature was controlled to study how polycarbonate responds to stress and bending. At around 147 °C, polycarbonate changes from being hard like glass to flexible like rubber because the material's stiffness

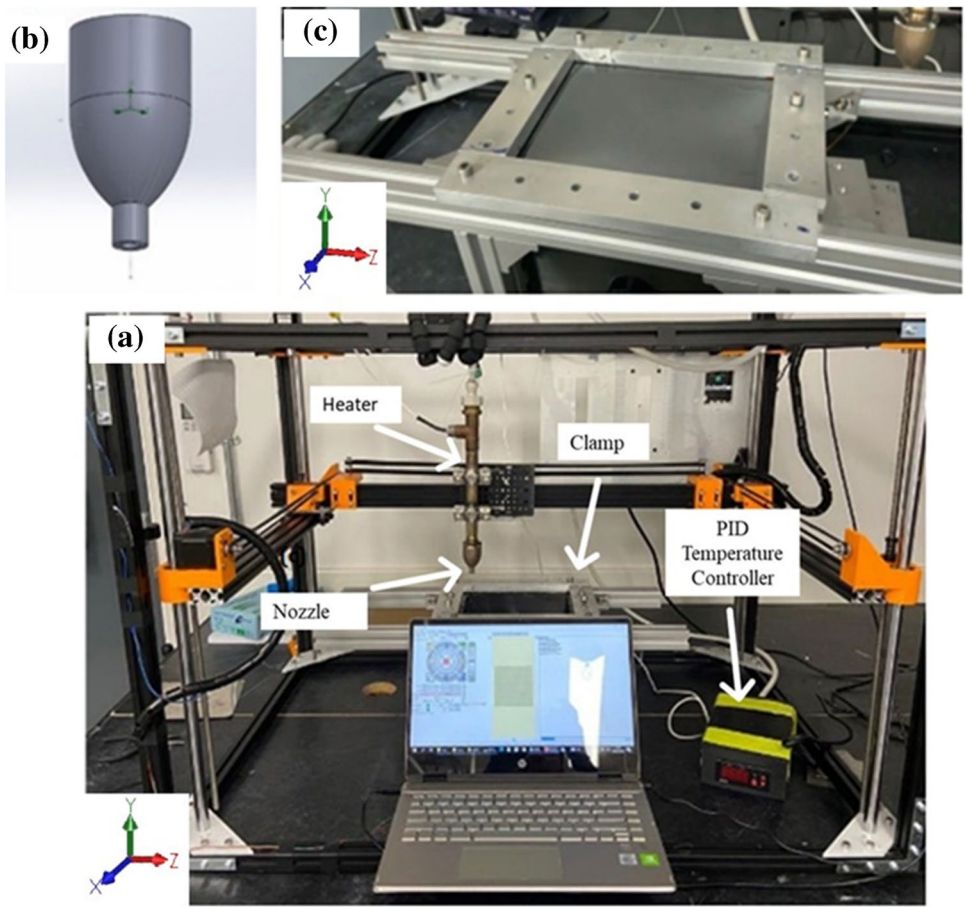

Fig. 1 **a** Full setup. **b** The forming tool. **c** Fixture for the PC sheet. Video: https://www.dropbox.com/s/w0n4n3narl0dgvi/Contact-less%20SPIF.mp4?dl=0

Table 1 Material properties of LEXAN® 9030 polycarbonate

Property	Value
Thickness	0.75 mm
Density	1.2 g/cc
Young's modulus	2.3 GPa
Yield stress	60 MPa
Poisson's ratio	0.38
Maximum elongation	110%
Thermal conductivity	0.2 W/m. °C

drops to zero at that temperature. This means that below 147 °C, it stays elastic, but above that, it starts to deform and behave more like plastic. A polycarbonate sheet with dimensions of $205 \times 170 \times 0.75$ mm^3 was prepared to perform the contactless SPIF experimental tests [21]. The forming operations were conducted at a tool speed of 0.75 m/min in the X and Z directions and 10 m/min in the Y direction for the step down movement (transition point). The initial distance between the nozzle and the sheet was 6 mm. Moreover, the truncated pyramid shape was generated so that 10 full loops were conducted, starting from a 152×120 mm^2 rectangle at the first loop and ending with a 62×30 mm^2 one in the last loop. The step down between consecutive loops was set to 0.75 mm for each step, with a total depth of 7.5 mm.

3 Simulation

To carry out the numerical simulation of the contactless SPIF method, ANSYS 21 Workbench software was employed in this study. In order to simplify the simulation for long tool paths, the sheet was treated as an isolated element, which entailed removing the frame used to secure the sheet. Additionally, a fixed support mechanical boundary condition was applied to the extremes of the sheet to maintain stability during the simulation. Notably, the support mesh results were not calculated to minimize the simulation time. A multilinear isotropic hardening material's engineering data were developed by defining the true stress and strain curves. Specifically, critical mechanical properties like the yield stress point were derived from literature [19, 20]. It is worth highlighting that changes in the tool used to conduct the process resulted in the integration of two different models into the software for the calculations. These two models will be explained in detail in the following subsections to provide a comprehensive understanding of the numerical simulation process.

3.1 Computational fluid dynamics

To investigate the compressed air pressure and temperature distributions and values produced by the nozzle design in the contactless SPIF process, a computational fluid dynamic model (CFD) using fluent from ANSYS software was utilized. As depicted in Fig. 2a, the simulation model consisted of three main parts: a reducer, a sheet, and a closed environmental box. The reducer was designed with a 33-mm inlet diameter, a 5-mm outlet diameter, and a height of 55 mm to control the temperature and pressure of the air flowing out from the heater. The temperature, pressure, flow rate, and of the air flowing towards the sheet were also analyzed. To model a deformed sheet, a polycarbonate sheet was included in the simulation under the nozzle outlet, positioned 6 mm away from the reducer nozzle. This allowed for the prediction of the pressure and temperature values reached on the top surface of the sheet during the forming process. Finally, a closed box was incorporated into the model to establish a closed environmental boundary, as depicted in Fig. 2a. This was essential to account for the effects of the surrounding environment during the forming process. The use of the fluent model allowed for a more in-depth analysis of the process and provided valuable insights into the performance of the new reducer design concept.

Regarding the meshing strategy for the CFD simulation, a hybrid mesh was created using a combination of structured and unstructured meshing techniques. The areas surrounding the nozzle and sheet were meshed with a relatively coarse element size of 1×10^{-3} m to minimize computational expense while still providing sufficient resolution to capture the overall flow behavior. However, in regions of high flow complexity, a finer mesh was necessary to accurately capture the details of the flow field. Therefore, a fine inflation mesh with 5 layers was implemented on the wall inside the nozzle and in the area between the nozzle and the sheet, with an element size of 1.5×10^{-6} m. This technique allows for a smooth transition between the coarse and fine meshes, ensuring that the numerical solution is accurately resolved across the entire domain. The mesh was created using a combination of commercial software tools and manual refinement to ensure optimal mesh quality and resolution. To provide a better understanding of the mesh employed in the study, a detailed figure (Fig. 2b) is included that shows the mesh structure and layout. The figure highlights the regions where the fine inflation mesh was used and demonstrates the smooth transition from the coarse to the fine mesh.

The viscous turbulence model k-ϵ is a widely used model in the field of computational fluid dynamics (CFD) that is designed to simulate turbulent flows. This model was employed in the analysis, with the aim of accurately predicting the behavior of the fluid being studied. The model is based on two transport equations, one for the turbulent kinetic energy k (see Eq. 1) and one for the turbulent dissipation rate ϵ (see Eq. 2). These equations are used to derive the rate of dissipation and kinetic energy of turbulence.

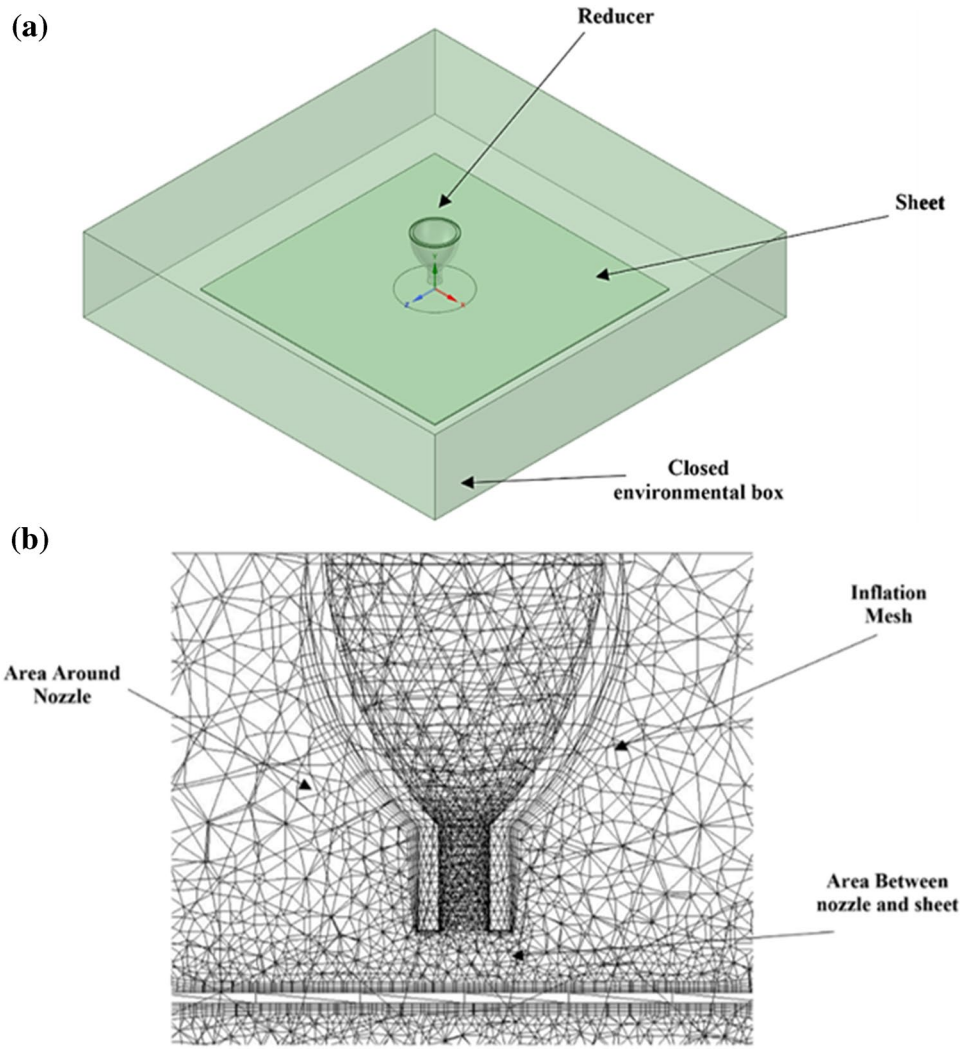

Fig. 2 **a** The three main components employed for the simulation of the CFD model. **b** The created mesh for the CFD model

The use of the k-ε model in FLUENT was first suggested by Launder and Spalding [22] and has since become a fundamental tool for actual engineering flow computations. Its accuracy and ability to provide reliable results for a wide range of turbulent flows make it an essential tool for engineers and scientists in many fields.

It is important to note, however, that the typical k-ε model is only applicable for completely turbulent flows. In other words, it may not be suitable for certain types of flows, such as laminar or transitional flows, and other turbulence models may need to be used in those cases. To simulate the behavior of the fluid accurately, the SIMPLEC algorithm was used in the simulation. This is a numerical method for solving the Navier–Stokes equations that is often used in CFD simulations. It is designed to provide accurate and reliable results while minimizing computational costs. The combination of the k-ε model and the SIMPLEC algorithm provided a powerful tool for analyzing and simulating turbulent flows. The equations governing the k-ε model, namely Eqs. 1 and 2, played a crucial role in accurately predicting the behavior of the fluid and ensuring the reliability of the results obtained [23, 24].

$$\frac{\partial}{\partial t}(\rho k) + \frac{\partial}{\partial xi}(\rho k u i) = \frac{\partial}{\partial xj}\left[\left(\mu + \frac{\mu t}{\sigma k}\right)\frac{\partial k}{\partial xj}\right] + Gk + Gb - \rho\varepsilon - YM + Sk \tag{1}$$

and

$$\frac{\partial}{\partial t}(\rho\varepsilon) + \frac{\partial}{\partial xi}(\rho\varepsilon u i) = \frac{\partial}{\partial xj}\left[\left(\mu + \frac{\mu t}{\sigma\varepsilon}\right)\frac{\partial \varepsilon}{\partial xj}\right] + C1\varepsilon\varepsilon k(Gk + C3\varepsilon Gb) + C2\varepsilon\rho\varepsilon 2k + S\varepsilon \tag{2}$$

where Gk is the kinetic energy of turbulence that is made by mean velocity gradients. Gb is the amount of kinetic energy that is added to turbulence because of buoyancy. YM is the amount that fluctuating dilatation in compressible turbulence adds to the overall rate of dissipation. $C1$, $C2$, and $C3$ are constants. σ_k and σ_ε and are the turbulent Prandtl numbers for k and ε, respectively. Sk and $S\varepsilon$ are source terms that were made by users.

In the simulation, time step increments were set to be steady, meaning that the time between each step remained constant throughout the simulation. This was done to ensure accurate and consistent results. To model the behavior of the air in the simulation, ideal gas properties were chosen for the air. The inlet air pressure was set to 1 bar, which is a measure of the air pressure at the inlet boundary. Additionally, the inlet temperature was set to 160 °C, which is the temperature at the inlet boundary.

3.2 Forming model

The second model aimed to analyze the deformation of the polycarbonate sheet. This was an important aspect to consider, as the final product needed to maintain its structural integrity under various conditions and achieve high quality geometrical precision. The model was created using ANSYS Parametric Design Language (APDL), which proved to be the most efficient way to represent the deforming tool, in this case, hot compressed air. The thermal element type SOLID226 was defined in the geometry section at the beginning of the model creation to allow the model to read the heat on the sheet. To simulate the path-moving design for the deformation, forty different coordinates in the X, Y, and Z directions were defined. An example of the tool path programmed for one experimental trial, see Fig. 3a, b. The sheet was meshed with a total of 12,141 elements to ensure accurate representation, see Fig. 3c. The movement of the hot pressure air over the plate occurred along the X and Z directions, while the step-down motion occurred along the Y direction, see Fig. 3e. In order to obtain accurate results, temperature-dependent polycarbonate material data were considered and assigned to the sheet.

According to the boundary condition, the sheet was assumed to be fixed at the edges, while the middle was free to deform. Additionally, the gravity force was taken into account and applied to the sheet to make it closer to the real case. The results of the hot compressed air from the fluent model were applied to the APDL commands. The pressure and temperature values obtained were displayed along the defined circle source. Furthermore, the specific path followed by the air source and nozzle was added to the model as a code following the coordinates previously determined. The air source, which had a diameter of 6 mm, was moved in the X and Z directions at a speed of 0.75 m/min. After one complete revolution, the step-down motion was simulated at a speed of 10 m/min in the X, Y, and Z directions to move the air source to the next step. After ten full paths with their corresponding steps were completed, the final shape of the sheet was calculated. This process was crucial in ensuring

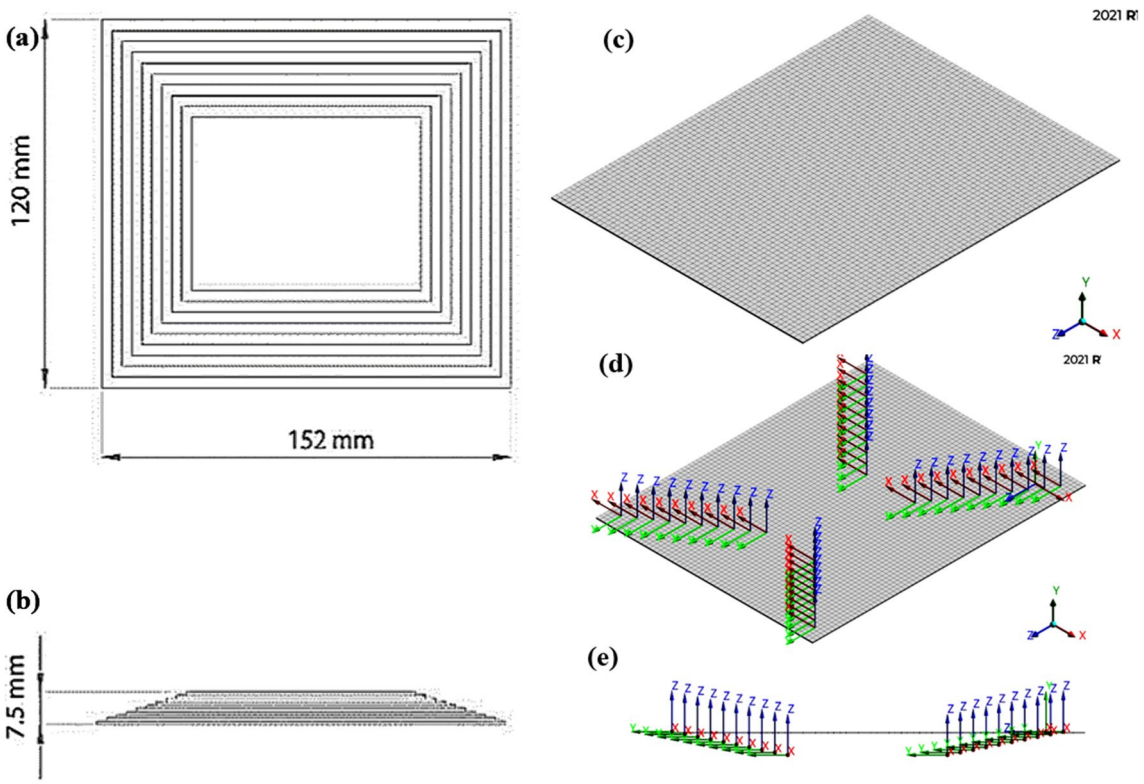

Fig. 3 Top view showing the tool tracks on the XZ plane (**a**) and side view showing the step downs in the Y direction (**b**), the developed mesh (**c**), the sheet X and Z coordinates (**d**), and sheet Y direction (**e**)

that the sheet would maintain its desired shape even under different conditions, and the model created allowed for accurate representation and analysis of the deformation process.

4 Results and discussion

4.1 Forming hot air motion

Figure 4 provides the CFD simulation of a detailed visualization of the compressed air pressure and temperature distributions along the radial direction on the polymer sheet as the air flows through the reducer channel and hits the polycarbonate sheet. The figure clearly shows the variations in pressure and temperature along the radial direction, providing important insights into the behavior of the fluid and the overall outcome of the simulation.

The pressure and temperature distributions are critical parameters to consider when analyzing the behavior of pressured hot air when passing over the polycarbonate sheet. The pressure distribution can influence the velocity and direction of hot air, while the temperature distribution can affect the thermodynamic properties of the air, such as density and viscosity, which in turn can impact the polycarbonate. As presented in Fig. 4a, b, the upper surface of the sheet reaches a pressure value of 0.078 MPa and a temperature of 154 °C. These values were employed as input for the second structural model utilized in this study.

4.2 Mesh sensitivity

The employed mesh sensitivity utilized elemental nodal forces to calculate the equivalent stress. To obtain a more stable model, a range number of elements was used to assess the effect of the elements number on the developed stresses and computing time, see Fig. 5a. The CPU time increased from 27 to 426 min when the number of elements increased from 2160 (coarse mesh) to 15,600 (fine mesh), respectively.

Despite the increase in CPU time, the accuracy of the equivalent stress calculation also improved with the

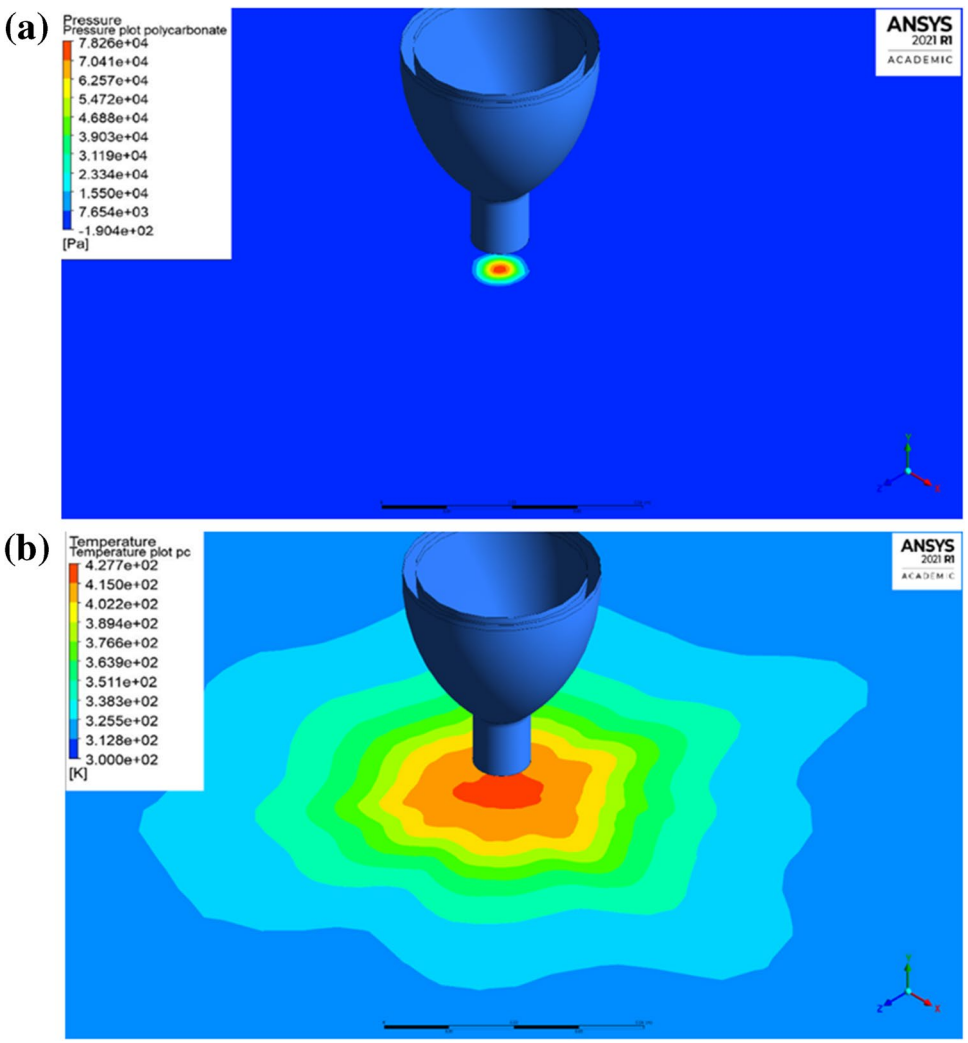

Fig. 4 **a** Pressure distribution. **b** Temperature distribution

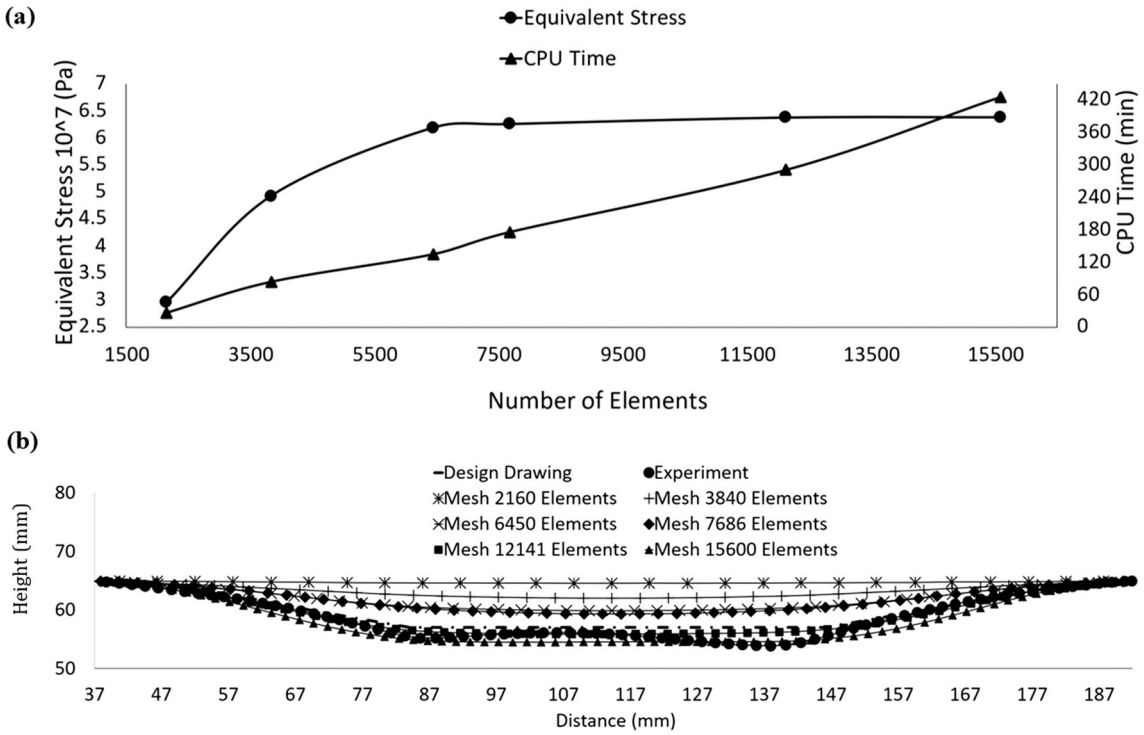

Fig. 5 Mesh Sensitivity (**a**) equivalent stress vs number of elements (**b**) comparison between FEM and experimental sheet profile

increasing number of elements (Fig. 5a). This demonstrates the importance of mesh sensitivity studies in accurately capturing the deformation behavior of the sheet and highlights the trade-off between computational efficiency and accuracy in FEM simulations.

As a result, it was determined that equivalent stress did not change significantly after 6450 elements and reached a stable mode at the 12,141 elements count. Since the mesh composed of 12,141 elements produced a stable result and increasing the number of elements over 12,141 increased the computational time without improving the precision of the model, the 12,141 elements mesh was chosen to be employed for evaluating the simulation results. Figure 5b illustrates a comparison between the predicted deformation values generated by the FEM and the actual deformation values measured from the experimentally formed sheet. By analyzing the agreement between the predicted and measured values, the accuracy of the simulation model can be evaluated.

To ensure that the results obtained from the finite element method (FEM) simulation accurately represent the experimental sheet profiles, the clamped workpiece was measured using a Mitutoyo Coordinate Measuring Machine Euro-CA776 (CMM). This allowed for the displacement boundary conditions specified in the FEM simulation to be replicated and matched to the displacement boundary requirements specified in the model and design drawing. The use of the CMM also eliminated any inaccuracies that may have occurred during unclamping and cooling, thereby enabling the effects of the new system to be seen more clearly. However, it was observed that the experimental profile shapes were significantly different from the simulated profiles when a coarse mesh was used (Fig. 5b). This discrepancy can be attributed to the fact that a coarse mesh cannot accurately capture the complex deformation behavior of the sheet.

4.3 Geometric profile

The model-predicted sheet final shape is seen in Fig. 4a. The simulation shows that successful sheet deformation can be achieved by employing the new contactless technique described in this study. Furthermore, Fig. 4b–d depicts a truncated pyramid part produced using the innovative contactless SPIF process. As shown, the profile obtained at 160 °C closely resembled the CAD design drawing profile, which demonstrates the effectiveness of the proposed technology. The contactless nature of the CIPF system ensures that there is no tool-to-sheet contact, which reduces the risk of damage to the sheet and extends the life of the tool. The figure also demonstrates visible surface texture differences and waviness. This illustrates the influence of the forming path on the part's surface and provides insight into the quality and accuracy of the formed part Fig. 6.

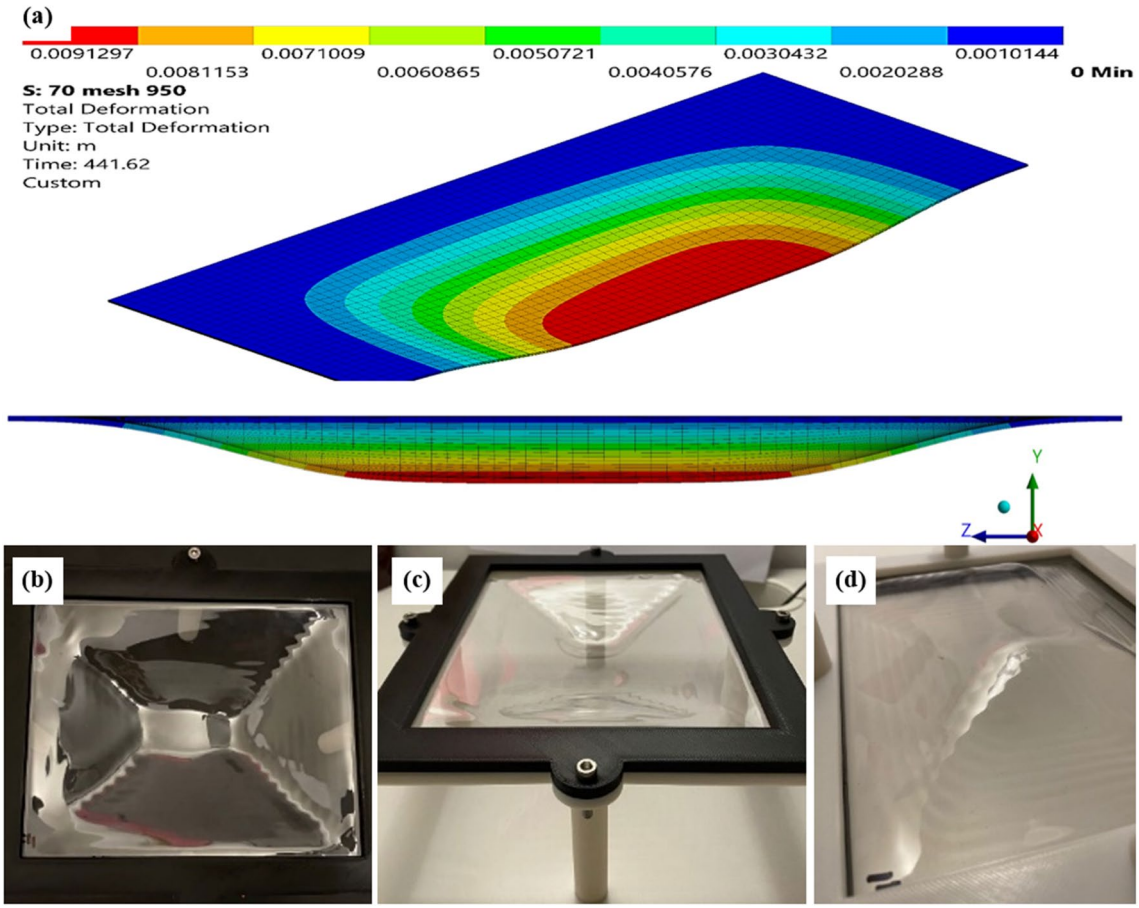

Fig. 6 **a** Sheet deformation results obtained by the model. **b–d** Images of the truncated pyramid part created in this work by using the contactless contactless SPIF process

Validation of simulation results was carried to ensure that the model accurately represents the physical system under investigation. In this study, CMM was used to measure the profile of the experimental result and compare it with the simulated and designed profiles. The CMM collected the "points cloud" of the formed truncated pyramid shape part that indicates the geometry of the workpiece. This allows for the computation of the profile and thickness of the deformed part, which can be compared with the simulation and design drawing data.

Figure 7 presents a comparison of the model-obtained profile, the experimentally measured profile, and the designed profile of the workpiece manufactured at 160 °C. To represent the model outcome, a cut section from the middle of the sheet was used, and the path from the workpiece edge to the center was determined using Ansys software.

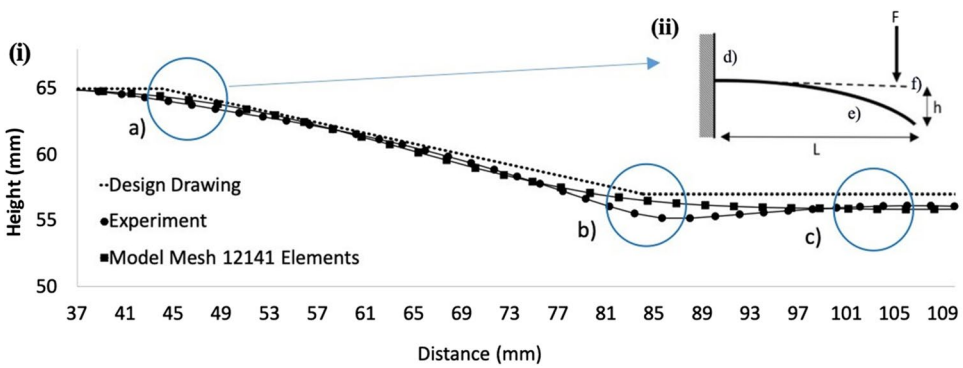

Fig. 7 **i** Comparison between model output, design drawing, and experimental profile. **ii** Bending effect at (d) edge of the sheet; (f) sheet before applying force; (e) sheet after applying force; (L) length from edge to starting point; (h) displacement from bending effect; (F) nozzle force position

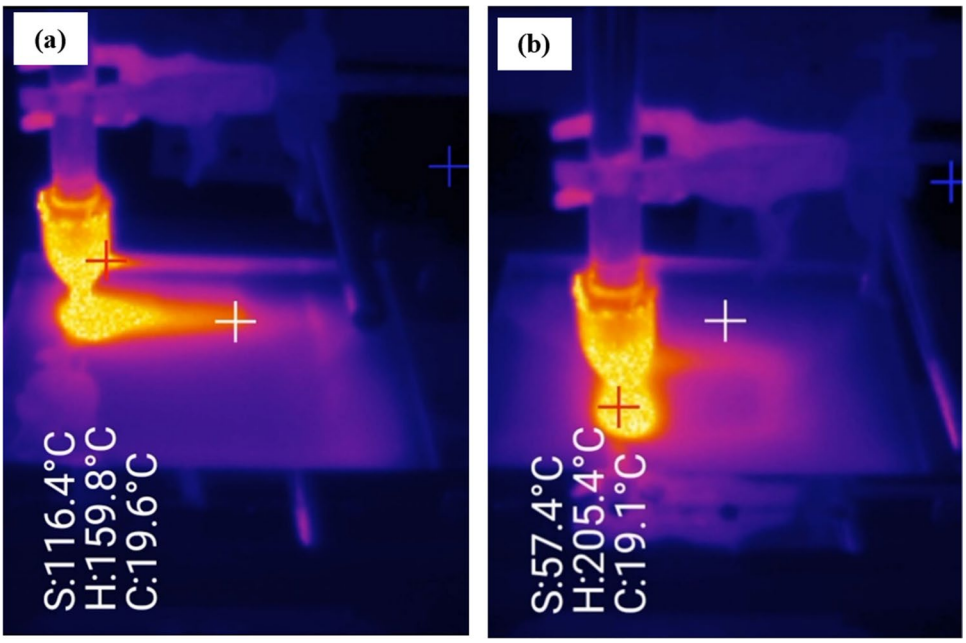

Fig. 8 Temperature tail at the first path (**a**) and last path (**b**) with tail overlapping. S, H, and C are representing surrounding, hot and cold spots, respectively

SolidWorks software was used to obtain the design drawing profile data, which included a path from the workpiece edge to the center.

The comparison of the profiles allows for a comprehensive analysis of the accuracy of the model. As presented in Fig. 7i, the FEM results is in a good agreement with the measured profile of the polycarbonate sheet. However, there are few areas (a–c) in the figure that shows discrepancies between the simulated and measured data, and the model can be improved upon to better represent the physical system.

In single point incremental forming (SPIF), the distance between the forming region and the sheet flange plays a critical role in determining the quality of the formed part. A narrow distance is preferred as it helps to minimize the bending impact at the major [25]. However, due to geometric limitations, the nozzle movement cannot be initiated from the sheet's original location, which generates a bending effect. This bending effect can impact the quality of the formed part, and therefore, it is essential to understand and minimize this effect. To better understand the bending effect, the horizontal and vertical displacements in deflection for a plastic sheet deformed by pressurized hot air and subjected to a vertical constant force and constant bending at the starting point of the nozzle was determined as (Fig. 7ii) [20, 22]. It was suggested that the distance between the fixed edge and the initial location of the nozzle should be minimized to reduce the bending effect. Additionally, other factors such as the sheet material properties, toolpath, and process parameters can also be optimized to minimize the bending effect and improve the quality of the formed part [26, 27]. The deformation between points (a) and (b) in Fig. 7i, follows a similar trend for the measured profile results in Fig. 7i. However, at the bottom corner in (b), the deformation for the model and the experiment profiles is greater than the designed one due to the high heating generated by the short path length, which causes the heat tail to overlap and the cooling to be extremely slow. The temperature distribution was measured using an RS T-10 smart thermal camera with 5% accuracy, and it was found that the temperature was eventually reaching 205 °C, see Fig. 8. Although the gas heater was calibrated to produce hot air at 160 °C, which was measured at the tip

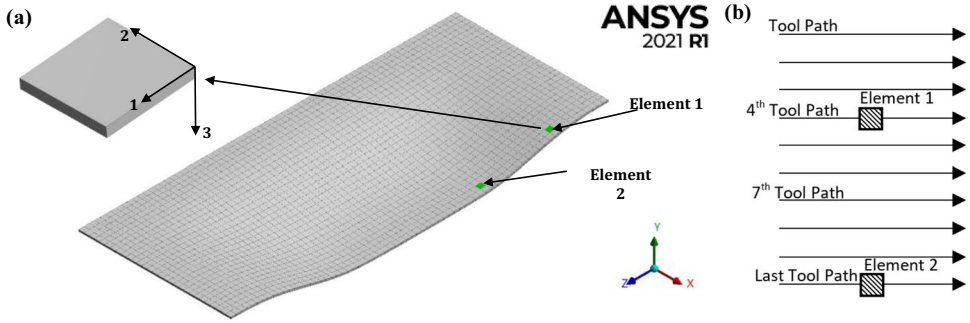

Fig. 9 **a** Selected elements along the cut profile wall. **b** Location of the selected elements in regard to the path number

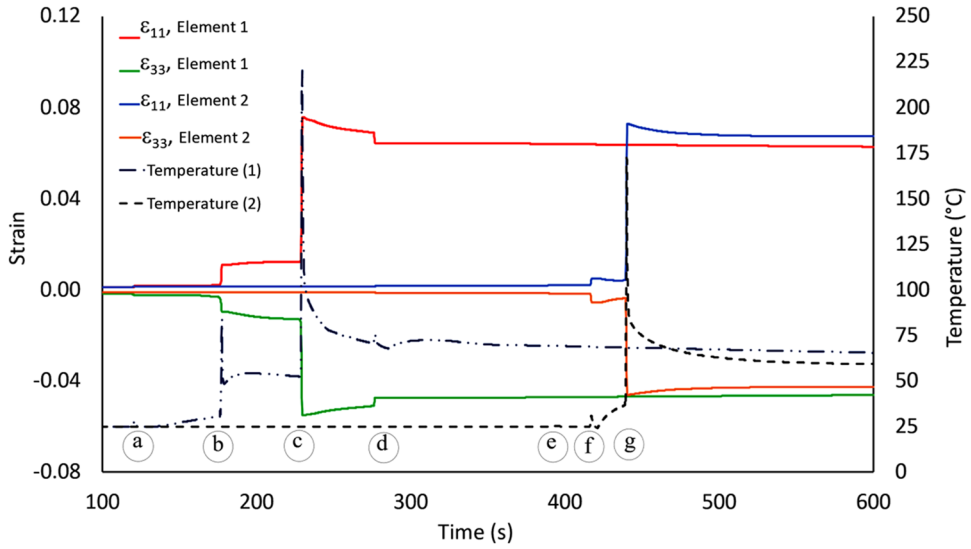

Fig. 10 Strain history on elements 1 and 2

of the nozzle. However, it is worth noting that during the deformation process, there was an unintended increase in temperature to 205 °C. This temperature elevation occurred in the final stage of the deformation process and was associated with a gradual reduction in the tool path, which in turn reduced the cooling time and resulted in this overheating. This overheating was addressed during the simulation by extrapolating behavior at higher temperatures. This extrapolation will be based on correlations established with the maximum temperatures reported in the relevant literature.

The study also observed minimal springback at the base of the pyramid, indicating that the process was able to accurately deform the polycarbonate sheet. However, a pillow effect was observed in the center as shown in (c) Fig. 7i, which could be attributed to the local heating of the sheet during the forming process [28]. The successful application of a hot compressed air tool has continued to improve the deformation process, and the developed numerical model is able to predict the deformations and the final shape of the PC sheet with very low mismatch. In fact, the acquired profile at 160 °C appears acceptably similar to the predicted and designed profiles.

4.4 Stretching and thinning

To investigate stretching and thinning of the polycarbonate sheet during the forming process, the history of the strain component of two control elements are chosen from the pyramid's upper surface was carried out (Fig. 9a): the former is situated in the middle, higher section of profile wall, while the latter is situated in the lower region, close to the pyramid's base. A local coordinate system is used to measure the strain components. It is important to note that Fig. 9b shows that elements 1 and 2 were on the fourth and the last path of the heating source, respectively.

The equivalent plastic strain analysis depicted in Fig. 10 provides insights into the stretching and thinning of the polycarbonate sheet during the forming process. The figure illustrates the strain components for directions 1 and 3, namely *ε11* and *ε33*, respectively, which have significant values in the 1–3 planes. As the heat source began to move, the sheet started to deform gradually, leading to the deformation process, which is explained in detail as follows:

At point (a), the heat source is on the second path and two steps-down from the first control element, causing a slight increase in temperature and strain. This trend continues as the source moves to the third path and one step-down from the first element at point (b), leading to a larger deformation compared to point (a).

At point (c), the source is on the same path as the first control element, resulting in a further increase in strain. However, after this point, the strain value decreases due to springback. At point (d), the source is one step further from the first element and heats it to 73.4 °C, causing it to reshape again. Although the temperature changes slowly in the range of ±4 °C, it does not affect the equivalent strain of element 1. The same effect can be seen at point (e), where the temperature increases by only 0.2 °C, causing a change in the equivalent strain at the second control

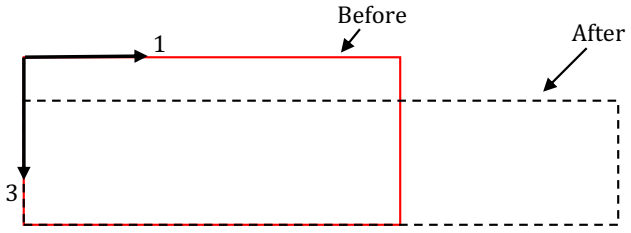

Fig. 11 Stretching and thinning phenomena on the elements

element. However, the amount of strain change is less than that observed at point (a).

At point (f), the source is one path before the second control element, and the strain amount is lower than that observed at point (b) due to material built-up at the bottom corner of the tool path, which reduces the strain of the element. At point (g), the source is on the same path as the second control element, and the strain value rises as shown at point (c) for element 1. However, there is no drop in strain as observed at point (d) since this is the last path of the tool, and the element is not heated with the air source again.

The strain grows gradually with the deformation of the elements. The major types of deformation during the proposed process are sheet stretching associated with $\varepsilon 11$, sheet thinning associated with $\varepsilon 33$, and sheet bending in the region adjacent to the sheet flange, as demonstrated in Fig. 11. These findings are consistent with previous studies by Hirt et al. [29] and Ambrogio et al. [30], which also reported the dominance of these deformation modes in SPIF. However, the employment of only two elements across the sheet is insufficient to acquire precise results on through-thickness shear strains. Several studies have aimed to tackle this problem by employing different methods of measuring strain, such as FEM, strain gauges, and digital image correlation. For instance, Mirnia et al. [31] used digital image correlation to measure the strain field during the SPIF process and reported that the maximum shear strain occurs in the flange region, which is consistent with the bending behavior observed in Fig. 11.

5 Conclusion and future work

In the present study, a novel contactless single point incremental forming (SPIF) process is presented, which utilizes innovative pressured hot air nozzle as a deforming tool for polymers forming. A finite element models was developed and implemented combine CFD and transient structural calculations to predict the deformation of a sheet under specific air pressure and temperature conditions. The CFD model is used to calculate the local distribution of the temperature and pressure of the air that hits the polycarbonate sheet, while the transient structural simulation is employed to calculate the deformation on the sheet. A truncated pyramid tool path is set, and an overall 7.5-mm depth track is simulated in 10 steps. To validate the model, the predicted sheet deformation is compared to the one generated experimentally, and the results obtained are in good agreement. The comprehensive FE model is able to predict the formed part geometries in addition to the normal strain progression. Moreover, it reveals that the primary modes of deformation in SPIF are stretching, thinning, and bending. Based on the results obtained, it can be stated that the model developed in this work is able to accurately predict sheet deformation generated through the contactless SPIF method proposed. The results of this study establish a solid groundwork for advancing and refining the contactless SPIF process. Furthermore, the use of additional polymer or low melting point metal materials could further enhance the process's potential for diverse applications in fields like automotive, aerospace, and biomedical engineering. This study's findings open up new avenues for exploring innovative designs and optimizing the contactless SPIF process to achieve superior outcomes in various applications.

Data availability All data generated or analyzed during this study are included in this published article.

Declarations

Ethical approval The authors confirm that this work does not contain any studies with human participants performed by any of the authors.

Conflict of interest The authors of this article declare that they have no conflicts of interest regarding the publication of this manuscript.

References

1. Dewang Y, Sheet SV (2023) metal shrink flanging process: a critical review of current scenario and future prospects. Mater Manuf 38:629–658. https://doi.org/10.1080/10426914.2022.2149779
2. Kopac J, Kampus Z (2005) Incremental sheet metal forming on CNC milling machine-tool. J Mater Process Technol 162-163:622–628. https://doi.org/10.1016/j.jmatprotec.2005.02.160
3. Chenghui Z, Feifei Z, Bo W, Yangjun L, Kai H, Ruxu D (2021) Digital twin-based stamping system for incremental bending. Int J Adv Manuf Technol 116:389–401. https://doi.org/10.1007/s00170-021-07422-7
4. Edwards WL, Grimm TJ, Ragai I, Roth JT (2017) Optimum process parameters for springback reduction of single point incrementally formed polycarbonate. Procedia Manuf 10:329–338
5. Zhu H, Ou H, Popov A (2020) Incremental sheet forming of thermoplastics: a review. Int J Adv Manuf Technol 111:565–587. https://doi.org/10.1007/s00170-020-06056-5
6. Silva MB, Martinho TM, Martins PAF (2013) Incremental forming of hole-flanges in polymer sheets. Mater Manuf 28:330–335. https://doi.org/10.1080/10426914.2012.682488
7. Durante M, Formisano A, Lambiase F (2019) Formability of polycarbonate sheets in single-point incremental forming. Int J

Adv Manuf Technol 102:2049–2062. https://doi.org/10.1007/s00170-019-03298-w
8. Martins PAF, Kwiatkowski L, Franzen V, Tekkaya AE, Kleiner M (2009) Single point incremental forming of polymers. CIRP Ann 58:229–232. https://doi.org/10.1016/j.cirp.2009.03.095
9. Franzen V, Kwiatkowski L, Martins PAF, Tekkaya AE (2009) Single point incremental forming of PVC. J Mater Process Technol 209:462–469. https://doi.org/10.1016/j.jmatprotec.2008.02.013
10. Kulkarni S (2016) Heat assisted single point forming of polymer sheets, 10. Kulkarni, S. Heat assisted single point forming of polymer sheets. In: computers and information in engineering conference. Charlotte, North Carolina, USA, V004T05A006. ASME. https://doi.org/10.1115/DETC2016-6003
11. Fontanari V, Benedetti M, Bruschi S, Fuganti A (2012) Numerical and experimental analysis of the single point sheets incremental forming process. In: The 15th International Conference on Experimental Mechanics, Porto, Portugal, p 12
12. Eksteen P, Van der Merwe A (2012) Incremental sheet forming (ISF) in the manufacturing of titanium based plate implants in the bio-medical sector. In: The 42nd International Conference on Computers and Industrial Engineering (CIE42), Cape Town, South Africa, 569–76
13. Thibaud S, Hmida RB, Richard F, Malecot P (2012) A fully parametric toolbox for the simulation of single point incremental sheet forming process: numerical feasibility and experimental validation. Simul Model Pract Theory 29:32–43
14. Abass K (2016) A study on using pre-forming blank in single point incremental forming process by finite element analysis. IOP Conf Ser: Mater Sci Eng 161:012031
15. Neto D, Martins J, Oliveira M, Menezes L, Alves J (2016) Evaluation of strain and stress states in the single point incremental forming process. Int J Adv Manuf Technol 85:521–534
16. Guzmán CF, Gu J, Duflou J, Vanhove H, Flores P, Habraken AM (2012) Study of the geometrical inaccuracy on a SPIF two-slope pyramid by finite element simulations. Int J Solids Struct 49:3594–3604
17. Araghi BT, Manco G, Bambach M, Hirt G (2009) Investigation into a new hybrid forming process: Incremental sheet forming combined with stretch forming. CIRP Ann 58:225–228
18. Gómez-López L, Miguel V, Martínez A, Coello J, Calatayud A (2013) Simulation and modeling of single point incremental forming processes within a solidworks environment, 2013. Procedia Eng 63:632–641
19. Richeton J, Ahzi S, Vecchio KS, Jiang FC, Adharapurapu RR (2006) Influence of temperature and strain rate on the mechanical behavior of three amorphous polymers: characterization and modeling of the compressive yield stress. Int J Solids Struct 43:2318–2335
20. Dar UA, Zhang W, Xu Y, Wang J (2014) Thermal and strain rate sensitive compressive behavior of polycarbonate polymer-experimental and constitutive analysis. J Polym Res 21:1–10
21. Fisher F, Brinson LC (2003) Macroscale experimental evidence of a reduced-mobility non-bulk polymer phase in nanotube-reinforced polymers. In: the 44th AIAA/ASME/ASCE/AHS/ASC Structures, Structural Dynamics, and Materials Conference, Norfolk, Virginia, 1702
22. Launder B, Spalding D (1974) The numerical computation of turbulent flows. Comput Methods Appl Mech Eng 3:269–289
23. Adanta D, Fattah IR, Muhammad NM (2020) Comparison of standard k-epsilon and sst k-omega turbulence model for breastshot waterwheel simulation. J Mech Eng Sci 7:039–044
24. Muralha A, Melo JF, Ramos HM (2020) Assessment of CFD solvers and turbulent models for water free jets in spillways. Fluids 5:104
25. Micari F, Ambrogio G, Filice L (2007) Shape and dimensional accuracy in single point incremental forming: state of the art and future trends. J Mater Process Technol 191:390–395
26. Borboni A, De Santis D (2014) Large deflection of a non-linear, elastic, asymmetric Ludwick cantilever beam subjected to horizontal force, vertical force and bending torque at the free end. Meccanica 49:1327–1336
27. Archansdran S, Shaari M, Rosly M (2016) Characterization of double layer IPMC bending actuation. ARPN J Eng Appl Sci 11:6536
28. Mohanraj Murugesan MS, Jung DW (2020) Experimental investigations on incremental sheet forming of commercial aluminum alloys for maximum production quality. Int J Mech Eng Robot Res 9:1264–1270
29. Hirt G, Bambach M, Junk S (2003) Modelling of the incremental CNC sheet metal forming process, In: The 10th International Conference on Sheet Metal, Newtownabbey, UK, 495–502
30. Ambrogio G, Filice L, Fratini L, Micari F (2004) Process mechanics analysis in single point incremental forming. AIP Conf Proc 712:922–927
31. Mirnia MJ, Shamsari M (2017) Numerical prediction of failure in single point incremental forming using a phenomenological ductile fracture criterion. J Mater Process Technol 244:17–43. https://doi.org/10.1016/j.jmatprotec.2017.01.029